Comparison of Stratus Cloud Properties Deduced from Surface, GOES, and Aircraft Data during the March 2000 ARM Cloud IOP

XIQUAN DONG,*,** PATRICK MINNIS,+ GERALD G. MACE,* WILLIAM L. SMITH JR.,+ MICHAEL POELLOT,# ROGER T. MARCHAND,@ AND ANITA D. RAPP&

*Meteorology Department, University of Utah, Salt Lake City, Utah
+NASA Langley Research Center, Hampton, Virginia
#University of North Dakota, Grand Forks, North Dakota
@DOE/Pacific Northwest National Laboratory, Richland, Washington
&Analytical Services and Materials, Inc., Hampton, Virginia

(Manuscript received 29 August 2001, in final form 14 June 2002)

ABSTRACT

Low-level stratus cloud microphysical properties derived from surface and Geostationary Operational Environmental Satellite (GOES) data during the March 2000 cloud intensive observational period (IOP) at the Atmospheric Radiation Measurement (ARM) program Southern Great Plains (SGP) site are compared with aircraft in situ measurements. For the surface retrievals, the cloud droplet effective radius and optical depth are retrieved from a δ2-stream radiative transfer model with the input of ground-based measurements, and the cloud liquid water path (LWP) is retrieved from ground-based microwave-radiometer-measured brightness temperature. The satellite results, retrieved from GOES visible, solar-infrared, and infrared radiances, are averaged in a 0.5° $\times$ 0.5° box centered on the ARM SGP site. The forward scattering spectrometer probe (FSSP) on the University of North Dakota Citation aircraft provided in situ measurements of the cloud microphysical properties. During the IOP, four low-level stratus cases were intensively observed by the ground- and satellite-based remote sensors and aircraft in situ instruments resulting in a total of 10 h of simultaneous data from the three platforms. In spite of the large differences in temporal and spatial resolution between surface, GOES, and aircraft, the surface retrievals have excellent agreement with the aircraft data overall for the entire 10-h period, and the GOES results agree reasonably well with the surface and aircraft data and have similar trends and magnitudes except for the GOES-derived effective radii, which are typically larger than the surface- and aircraft-derived values. The means and standard deviations of the differences between the surface and aircraft effective radius, LWP, and optical depth are $-4\% \pm 20.1\%$, $-1\% \pm 31.2\%$, and $8\% \pm 29.3\%$, respectively; while their correlation coefficients are 0.78, 0.92, and 0.89, respectively, during the 10-h period. The differences and correlations between the *GOES-8* and aircraft results are of a similar magnitude, except for the droplet sizes. The averaged GOES-derived effective radius is 23% or 1.8 μm greater than the corresponding aircraft values, resulting in a much smaller correlation coefficient of 0.18. Additional surface–satellite datasets were analyzed for time periods when the aircraft was unavailable. When these additional results are combined with the retrievals from the four in situ cases, the means and standard deviations of the differences between the satellite-derived cloud droplet effective radius, LWP, and optical depth and their surface-based counterparts are $16\% \pm 31.2\%$, $4\% \pm 31.6\%$, and $-6\% \pm 39.9\%$, respectively. The corresponding correlation coefficients are 0.24, 0.88, and 0.73. The frequency distributions of the two datasets are very similar indicating that the satellite retrieval method should be able to produce reliable statistics of boundary layer cloud properties for use in climate and cloud process models.

1. Introduction

Clouds are the dominant attenuators of radiation in the atmosphere, yet they remain one of the more uncertain quantities in climate models. To improve our understanding of the radiative interactions between the surface, clouds, and other atmospheric components and to obtain long-term records of relevant radiation data, the Department of Energy (DOE) Atmospheric Radiation Measurement (ARM) program (Stokes and Schwartz 1994) established the ARM Southern Great Plains (SGP) site (36.6°N, 97.5°W) in 1993. One of the primary purposes of the ARM program is to improve the representation of radiation and clouds in general circulation models (GCMs) using the ground-based observations. Because they can be used to define the radiation field and the distribution of condensed or frozen cloud water, cloud properties, such as cloud droplet effective radius (r_e),

** Current affiliation: Department of Atmospheric Sciences, University of North Dakota, Grand Forks, North Dakota.

Corresponding author address: Dr. Xiquan Dong, Department of Atmospheric Sciences, University of North Dakota, 4149 Campus Rd., Clifford Hall 400, Box 9006, Grand Forks, ND 58202-9006.
E-mail: dong@aero.und.edu

optical depth (τ), and liquid water path (LWP) are critical links between the atmospheric hydrological cycle and the radiation budget. Accurate representation of both hydrological and radiative processes should yield improved climate prognostications. Surface-based datasets can be used to measure these parameters continuously, but only provide a view from one side of the clouds and sample a small portion of the atmosphere directly over the site. To complement the surface measurements and bound the radiation budget at the top of the atmosphere (TOA), ARM also supports a satellite data analysis effort (e.g., Minnis et al. 1995b) to derive cloud properties and radiative fluxes from measured satellite radiances. Cloud and radiative parameters in climate models should be comparable to those that are observed from long-term satellite and surface observations.

For reliable application of satellite datasets in cloud processes and climate models, it is important to have a reasonable estimate of the errors in the derived cloud and radiative properties. The ground-based measurements can provide a baseline for estimating errors in the satellite products, however the ground-based measurements must be properly analyzed and validated and their uncertainties must be understood before they serve as a baseline. The comparisons between the ground- and satellite-based observations must be conducted carefully because of significant spatial and temporal differences between the two different observing platforms. Also because clouds are so variable, a statistically reliable validation requires coincident satellite-surface measurements taken in a variety of conditions. Comparisons with aircraft in situ measurements are critically needed to quantify the uncertainties in ARM ground- and satellite-based measurements and retrievals of cloud properties. The general approach to validate climate model results from the observations is as follows: aircraft in situ measurements are used to validate the retrievals from various algorithms applied to the ground-based observations (Dong et al. 1998), then the validated ground-based data are used to verify satellite results (Dong et al. 2001), and finally the large-scale satellite data are used to validate climate model simulations (e.g., Wielicki et al. 1995). Although other approaches for validation (e.g., Minnis et al. 1993; Platnick and Valero 1995; Dong et al. 2001) are also important, they are only case studies and cannot provide the statistical database resulting from long-term, continuous measurements over a variety of sites in various climatic regimes. The general approach of the validation effort is a long-term process that involves many different experiment and analysis teams. This paper focuses on one aspect of the validation process: continental stratus clouds.

During March 2000, the ARM program conducted an intensive observational period (IOP) at the ARM SGP site to obtain comprehensive ground- and satellite-based measurements of clouds in conjunction with flights of the University of North Dakota Cessna Citation research aircraft. One of the goals of this IOP was to validate ground- and satellite-based retrievals of r_e, τ, and LWP using aircraft in situ measurements. This paper reports the results of four continental stratus cloud cases (hereafter the four in situ cases) that were intensively observed by the ground- and satellite-based remote sensors and aircraft in situ instruments during 3, 17, 19, and 21 March. The comparison of these results provides more data for assessing the uncertainties in the remotely sensed parameters from both surface and satellite over the ARM SGP site. Three additional cases without aircraft data are also examined.

2. Data and methods

a. Surface

Dong et al. (1997, hereafter D97; 1998; 2000) demonstrated that the combined measurements from the ground-based cloud radar, ceilometer, microwave radiometer (MWR), and standard Eppley precision spectral pyranometers (PSP; 0.3 to 3 μm) provide the basic information needed to study the stratus cloud properties. This information includes cloud boundaries, LWP, and solar transmission at the surface. To retrieve the microphysical and radiative properties of stratus clouds, D97 used a δ2-stream radiative transfer model in conjunction with ground-based measurements. The retrieved cloud properties include the layer-mean cloud-droplet effective radius (r_e), broadband shortwave optical depth (τ), and TOA albedo (R_{TOA}). The retrieval scheme is based on an iterative approach that varies r_e in the radiative transfer calculations until the model-calculated solar transmission matches the measured value. The uncertainties in τ and R_{TOA} are generally less than 5%, while in r_e is about 10%, which is mainly contributed by the ''expected'' errors of surface measurements in cloud LWP and solar transmission (D97; Dong et al. 1998).

The cloud-top height is derived from cloud radar reflectivity profile, and the cloud-base height is derived from the Belfort laser ceilometer that can detect high densities of small cloud droplets and provides more precise cloud base heights than cloud radar because cloud radar often detects precipitation-sized particles below cloud base. The vertical resolutions of radar-derived cloud top height and ceilometer-derived cloud-base height are 45 and 8 m, respectively. The cloud LWP is retrieved from the MWR brightness temperatures measured at 23.8 and 31.4 GHz using a statistical retrieval method (Liljegren et al. 2001). The rms accuracies of the retrievals are about 20 g m^{-2} and 10% for cloud LWP below and above 200 g m^{-2}, respectively (Dong et al. 2000; Liljegren et al. 2001).

The ground-based measurements are averaged to 5-min resolution to have better correlations between them. The surface retrieval technique uses data from a cylinder of cloud directly above the ground-based instruments. For a cloud layer with base and top heights of 0.5 and 1 km, the broadband and hemispheric field-of-view

PSPs sample most of solar transmission from a circular area of radius equal to cloud-base height, centered directly above the pyranometer (Dong 1996). The MWR has a nominal field of view of 5°, and the beamwidth of cloud radar is 0.24°. For a typical low-level stratus cloud, its wind speed is about 10 m s^{-1} (notice that this may vary cloud by cloud); the cloud will advect about 3 km in 5 min. The 5-min sample volumes for the MWR and cloud radar are nearly the same, which is the product of 3 km and cloud geometric thickness, while the PSP samples an even larger volume because of its hemispheric field of view, but most of its sampled volume has an overlap with the MWR and cloud radar sampling. The real sampling volumes from different instruments are dependent on their field-of-view angles, wind speed, and cloud-base height. We find that there are good correlations between the surface measurements and reasonable retrievals in 5-min temporal resolution (D97).

b. Satellite

Cloud and radiation parameters derived from half-hourly, 4-km radiances taken by the *eighth Geostationary Operational Environmental Satellite* (*GOES-8*, hereafter GOES) during the IOP are compared with the ground-based observations and aircraft in situ measurements. The GOES radiances were calibrated by Minnis et al. (2002) using collocated measurements from the Tropical Rainfall Measuring Mission (TRMM) Visible Infrared Scanner (VIRS). Cloud temperature T_c, visible (VIS; 0.65 μm) optical depth, r_e, and LWP were derived by Minnis et al. (2001) from the multispectral GOES imager data using the visible infrared solar infrared split-window technique (VISST), an updated version of the three-channel technique described by Minnis et al. (1995a, see their Figs. 4.3–10). VISST relies on the infrared (IR; 10.8 μm) radiance to determine cloud temperature, the visible reflectance to obtain cloud optical depth, the solar infrared (SI; 3.9 μm) radiance to estimate cloud particle size, and the split-window channel (SWC; 12.0 μm) to help determine phase (Young et al. 1997). These parameters are determined iteratively for each pixel by matching the observations with a set of theoretical calculations with estimated instantaneous uncertainties of 15% for r_e and 12% for τ.

As a precursor to the VISST, the data are initially analyzed with the VIS–IR layer bispectral threshold method (LBTM; see Minnis et al. 1995b) to provide default solutions for every pixel that serve as initial values in the VISST iteration. The VISST computes a set of radiances for all four wavelengths over a range of optical depths and effective ice crystal and water droplet sizes given the viewing and illumination angles and a profile of temperature and humidity. The computations use a set of cloud SI, IR, and SWC emittance parameterizations and VIS and SI reflectance lookup tables (Minnis et al. 1998) in simplified radiative transfer models of the atmosphere (Minnis et al. 1993). The radiative transfer parameterizations incorporate the estimated clear sky radiances for each channel and detailed atmospheric absorption parameters based on the correlated *k*-distribution method developed specifically for the GOES filter functions. The computational results are used iteratively to match the theoretical results for the VIS, SI, and IR channels with their measured counterparts to find a solution for ice and liquid water clouds separately. Thus $T_{\rm cw}$, τ_w, and r_e are found for liquid water, and $T_{\rm ci}$, τ_i, and effective diameter D_e are determined for ice, if possible, respectively. The final solution is chosen using the following logic.

Often, a solution cannot be obtained for one of the phases because most ice clouds are not as reflective as most water droplet clouds at SI wavelengths (e.g., Minnis et al. 1998). If only the ice solution is obtained and $T_{\rm ci} < 273$ K, then $T_c = T_{\rm ci}$, and $\tau = \tau_i$; otherwise, it becomes a no-retrieval pixel. Similarly, if only the water solution is found and $T_{\rm cw} > 233$ K, then $T_c = T_{\rm cw}$, and $\tau = \tau_w$. Otherwise, it is classified as no retrieval, and the default LBTM value is used or it is reclassified as a clear pixel. These checks provide phase classifications for nearly 75% of pixels.

In certain angular conditions and at some optical depths or in mixed phase or multilayered cloud conditions, model results overlap giving two solutions (e.g., Minnis et al. 1995a; Minnis et al. 1998). When two solutions are found, then the ice solution is used if both $T_{\rm cw}$ and $T_{\rm ci}$ are less than 233 K. If both temperatures are greater than 273 K, then the water results are selected. For the remaining conditions, the SWC brightness temperature $T_{\rm SWC}$ is computed for the two cloud results. If the two values differ by more than 2.5 K and the brightness temperature difference between the IR and SWC calculations exceeds 1 K for at least one of the phases, then the phase is selected based on the computed value of $T_{\rm SWC}$ closest to the observed value. If no phase selection results, then a decision process is employed that is based on the LBTM height classification. For pixels classified as high clouds by the LBTM, the ice solution is chosen if the coldest pixel in the high-cloud layer is colder than the coldest pixel in the low-cloud category and $T_{\rm ci} < 273$ K. For LBTM low-cloud pixels, the water solution is selected if $T_{\rm cw} > 233$ K and $r_e < 20$ μm. For midlevel LBTM cloud pixels, the ice solution is selected if $T_{\rm ci} < 273$ K and $D_e > 45.3$ μm. Water is chosen if $T_{\rm cw} > 233$ K and $r_e < 23$ μm. Finally, if no decision was forthcoming from the LBTM checks, then water is selected if $T_{\rm cw} > 253$ K; otherwise the ice solution is selected.

Cloud LWP is then computed from the combination of the retrieved τ and r_e as in Minnis et al. (1998). TOA broadband albedo ($R_{\rm TOA}$) was computed from the GOES narrowband albedo using an empirical relationship based on a correlation between coincident October 1986 *GOES-6* and Earth Radiation Budget Experiment (ERBE) satellite data (Minnis and Smith 1998). The narrowband albedo is simply the observed visible re-

flectance corrected for anisotropy using a bidirectional reflectance model (Minnis et al. 1995b). Means and standard deviations were computed for each parameter using all of the pixels (~150) within a 0.5° × 0.5° box centered on the SGP central facility (SCF) in 30-min temporal resolution. This box size was used to simplify the comparisons because this type of approach will be used for long-term datasets. Exact matching of pixels with surface or aircraft observations is a time-consuming process and fraught with its own uncertainties. Each of the surface measurements that are used in a single retrieval of size, optical depth, and LWP is taken from a different field of view. The radar and ceilometer observe a small beam that maps out a tiny cross section of the cloud passing overhead, while the MWR observes a larger cone that increases with increasing height. The shortwave radiometer is a hemispherical instrument that measures radiation from a much larger area than the other instruments. Its field of view grows rapidly with cloud-base height. Thus, exact matching of the satellite pixels with the surface data must account for cloud-base height and wind speed while making some compromise that minimizes the uncertainties in the areas viewed by the different surface instruments. The use of the means and standard deviations within a 0.5° box allows for a reasonably simple comparison of the spatial statistics of the cloud fields with the temporal statistics generated from the surface data. This assumption is examined later.

Means were also computed separately for ice and water cloud pixels. The phase determination is generally reliable for single-layered clouds. However, when a thin cirrus cloud overlays a thick low-level cloud, phase detection becomes ambiguous because all of the spectral radiances are influenced by both cloud layers. Ice clouds generally decrease the amount of reflected SI radiation relative to that for a water cloud. This effect can result in either a large value for r_e or a small value of ice particle size depending on the final phase classification (Kawamoto et al. 2001). Han et al. (1994) showed that an optically thin cirrus cloud over a stratus cloud with $r_e = 10$ μm can cause a dramatic overestimate in the retrieval. For example, for an ice cloud optical depth of 0.5, the retrieved value was 5 μm greater than the true value. Classification of overlapped pixels would remove the uncertainty associated with their effects. Although some methods have been developed to detect overlapped clouds (e.g., Ou et al. 1996), none are available for the specific channels used here. Those that are available have only been demonstrated for limited case studies.

To minimize the impact of ice clouds on the retrievals, some of the potential comparisons were eliminated. Using the radar as a guide to the presence of cirrus, all satellite results that had more than 30% ice cloud retrievals were eliminated. Results with a standard deviation in r_e exceeding 3 μm were also eliminated if between 1% and 30% of the pixels were classified as ice or the radar indicated the presence of some cirrus clouds. These thresholds were used to include those samples that had clearly separated cirrus-covered and cirrus-free areas as well as those that included relatively thin cirrus that would have minimal impact on the retrievals. This screening eliminated seven and two 30-min samples on 3 and 21 March, respectively, and all of the potential comparisons on 16, 18, and 22 March. Remaining overlapped cases, such as 17 and 21 March, appeared to have little effect on the results as discussed later.

c. Aircraft

The University of North Dakota Citation research aircraft carried several Particle Measuring Systems (PMS) probes to measure cloud microphysical properties in situ at a 4-Hz sampling rate. Cloud droplet spectra measured with a PMS Forward Scattering Spectrometer Probe (FSSP-100) were averaged to 1 Hz for this study. The FSSP probe sized and counted individual particles in 15-diameter bins, with bin centers from 4.4 to 52.3 μm. Corrections to particle concentrations were applied to account for probe activity and coincidence (electronic dead time; see Baumgardner et al. 1985) and for variations in the effective beam diameter (Dye and Baumgardner 1984). Particle size corrections to account for electronic response time and beam inhomogeneity follow Baumgardner and Spowart (1990). The sizing correction scheme redistributes the counts into new bins requiring adjustment of the bin widths to account for ambiguities in the Mie scattering curve. Cloud liquid water content (LWC) was calculated from each FSSP spectrum, and r_e was computed as the ratio of the third to the second moment of the cloud particle size spectrum. Cloud LWP was deduced from the FSSP-measured LWC and ground-based radar and lidar-measured cloud geometric thickness (recognizing that uncertainties exist in this approach due to vertical variability in LWC), and τ was then derived from the ratio of LWP to r_e. Given the aircraft speed of 85 m s^{-1} for low-level stratus operations during the IOP, the aircraft traveled about 25 km of distance in 5 min and typically traveled through the depth of the cloud layer at least once during this time period. Thus, the 5-min cloud LWP and τ values derived from the aircraft data represent a reasonable vertical and horizontal average of the cloud properties over the site area.

Based on the previous studies (e.g., Baumgardner 1983; Dye and Baumgardner 1984; Baumgardner et al. 1985), Miles et al. (2000) summarized all possible errors for FSSP measurements. They are 1) inhomogeneity across the length and width of the laser beam, which introduces sizing errors; 2) a limited response time in the detector electronic, which can lead to considerable underestimates of cloud droplet number concentration (N); 3) coincident counts, which may underestimate N and overestimate r_e; 4) the propagation of error from particle concentrations and size to volume estimates, which can lead to large error to LWC; and 5) uncertainties associated with the calibration technique. The

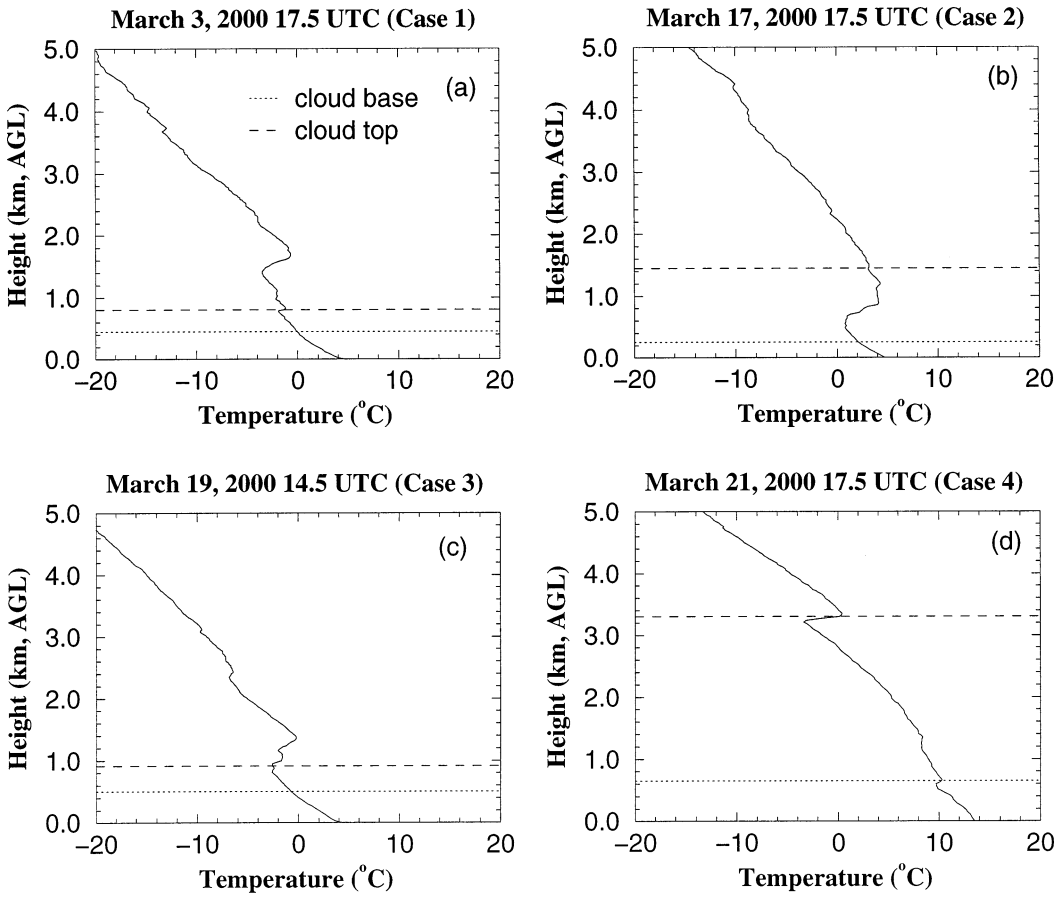

FIG. 1. Temperature soundings for the four in situ cases and the radar-derived cloud-top height (dash) and ceilometer-measured cloud-base height (dot) at the ARM SGP site during the IOP.

overall uncertainties in r_e, N, and LWC are 14%, 25%, and 30%, respectively, when all possible corrections are made to the measurements.

In the four in situ cases, the mean values of cloud-base and -top heights derived from ground-based radar and ceilometer measurements are 624 and 1581 m, respectively, and the mean LWC from FSSP measurements is 0.205 g m^{-3}. The mean LWP (196 g m^{-2}) is the product of surface-derived cloud geometric thickness (957 m) and FSSP-derived LWC (0.205 g m^{-3}). The vertical resolutions of cloud-base and -top heights are 8 and 45 m, respectively, which results in the uncertainty of ~50 m in cloud geometric thickness. This uncertainty only causes about 6% (=53/957) error in deriving cloud LWP if the FSSP-derived mean LWC is used, while 30% uncertainty in FSSP-derived LWC will lead to the same percentage of error in cloud LWP. Since cloud optical depth is derived from the ratio of cloud LWP and effective radius, its uncertainty is nearly the same as or slightly larger than cloud LWP.

3. Results and discussion

Four low-level stratus cases (the four in situ cases on 3, 17, 19, and 21 March) were intensively observed by the ground- and satellite-based remote sensors and aircraft instruments resulting in a total of 10 h of simultaneous data from the three platforms. Three additional stratus cases during the IOP (14, 15, and 29 March) were observed from the ground- and satellite-based remote sensors only. Figure 1 plots the soundings from the radiosondes launched nearest to the aircraft flight times. Also noted in Fig. 1 are the approximate cloud top and base heights for each of the cloud cases. Since the cloud temperatures for the four in situ cases were around or greater than 0°C, it is assumed that no ice was present in the clouds. The Citation flight tracks for each day are shown in Fig. 2 in terms of the aircraft distance from the SCF. A portion of each flight was spent directly over the SCF.

The large-scale context for the four in situ cases can be seen in the pseudocolor GOES imagery in Fig. 3. These images, created by using the visible, solar infrared, and infrared radiances to determine the intensities of red, green, and blue, respectively, are convenient for showing most of the information that normally requires two or three images to convey. Clear areas are primarily green and brown, while cloudy areas are various shades of yellow, orange, pink, and white. Because they atten-

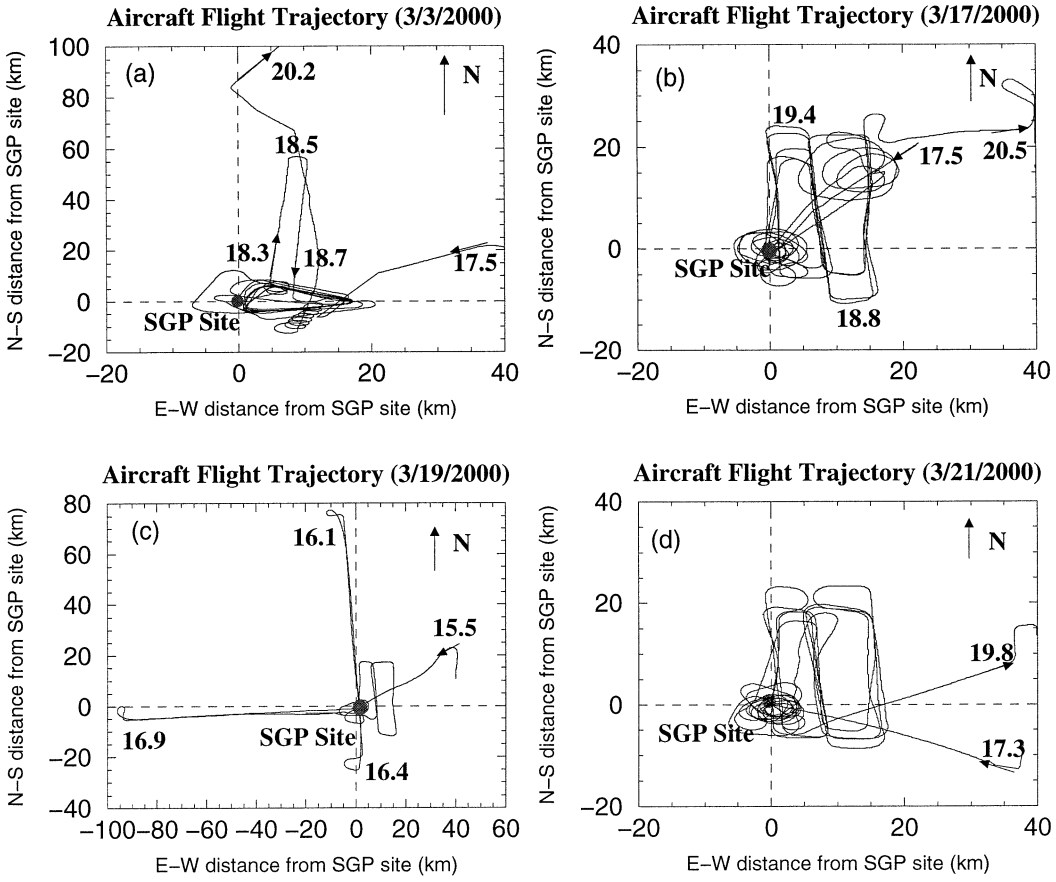

FIG. 2. Citation flight tracks relative to the ARM SCF during the Mar 2000 cloud IOP.

uate the radiation in all three channels at nearly same relative amounts, thin cirrus clouds are white over cloud-free backgrounds. Thin cirrus over low clouds or thick cirrus are pink or light magenta because the large ice crystals absorb most of the incoming solar infrared radiation, while the cloud has a low infrared temperature and a large visible reflectance. Liquid water clouds are yellow or orange. The areas of deep magenta are cloud-free snow-covered regions.

a. Case 1, 3 March

The satellite imagery at 19.3 (hours) UTC for case 1 (Fig. 3a) suggests that cirrus clouds are northwest and east of the SGP site. The ground-based radar observations (not shown) also reveal the presence of cirrus clouds before 17.5 and after 21.5 UTC. Only data taken between 17.5 and 21.5 UTC (local noon is 18.5 UTC) were used for this case to minimize contamination of the satellite and surface measurements by cirrus clouds over the low-level stratus clouds. The sounding from 17.5 UTC shows a northerly wind of $\sim$15 m s^{-1}. The cloud is under the lowest inversion at a temperature around 0°C (Fig. 1a). The aircraft remained within 20 km of the SCF flying a triangular pattern over several additional remote sites distributed in a small array northeast and east of the SCF (Fig. 2a). Early in the flight, the Citation flew towards the SCF from the northeast, then slowly descended from cloud top to cloud base and quickly climbed back to cloud top in the triangle pattern. Around 18.3 UTC, the aircraft flew northward from the SCF in the middle of cloud and returned to the SCF from the northeast at 18.7 UTC. It then repeated the triangle pattern, used at the beginning of the flight, until 20.0 UTC.

As shown in Fig. 4, the ceilometer-measured cloud base was near 0.5 km, while the radar-derived cloud-top height varied from 1 to 1.5 km during the 4-h period. The excellent agreement in r_e between the surface retrievals and aircraft data suggests that, during the 5-min averaging period, the aircraft probes collected enough samples to match the scales being characterized by the averaged surface-based data. The means on the right side of Fig. 4 represent the averaged values when all three datasets are available, such as from 17.5 to 20.0 UTC. The effective radii derived from GOES have the same trend as the surface and aircraft data. However, the satellite-derived effective radii are larger than those retrieved from both the ground-based data and the aircraft in situ measurements. The small differences could

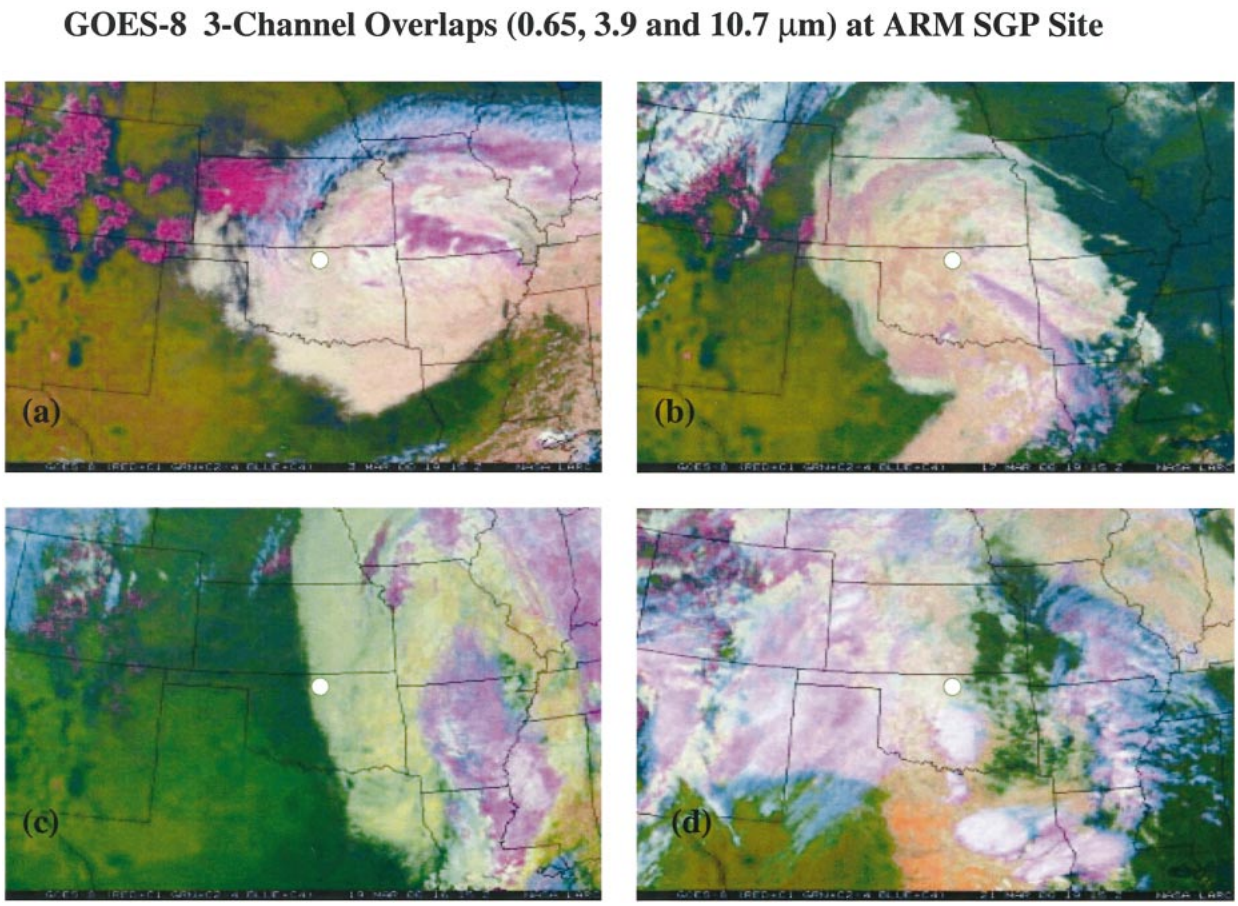

FIG. 3. GOES three-channel composite images at the ARM SGP site (white circle) at (a) 19.25 UTC, 3 Mar 2000, (b) 17, (d) 21, and at (c) 16.25 UTC, 19 Mar 2000. White and light pink colors represent high and ice clouds, and yellow and orange represent low and liquid clouds.

arise for several reasons. Because GOES samples a different area than either the surface or aircraft, the average may be slightly biased. Sampling is probably a factor prior to 20.0 UTC given that r_e from either the aircraft and/or the surface is within one standard deviation of r_e from GOES. Residual cirrus contamination might have affected some of the results between 19.5 and 21.5 UTC. Although T_c varied from 270.2 to 271.1 K, no ice-cloud pixels were detected between 17.5 and 19.5 UTC. A few were found after 19.5 UTC, when the mean value of T_c decreased and the standard deviation of T_c increased. Cirrus contamination (see case 2 for a discussion) might have contributed to the divergence in Fig. 4 between the VISST and surface-derived values of r_e after 19.5 UTC. Close examination of the 1-km VIS data, however, reveals a thinning of the clouds in the box and some possible breaks in the cloud field resulting in partially cloud-filled 4-km pixels. Errors in the prescribed surface skin temperature could result in errors in r_e for the thin clouds, while partially cloud-filled pixels cause an overestimation of r_e.

All of the differences, especially those seen prior to 19.5 UTC, are probably due to mostly to the sensitivity of the satellite retrieval to the conditions at cloud top. As shown by Nakajima and King (1990) and Platnick (2000), the retrieval of effective droplet size using 3.7-μm data is typically biased high in optically thick stratus clouds because the reflected solar radiation emanates mostly from the larger droplets near the top of the cloud. The solar radiation is generally absorbed or reflected before it can reach the lower layers that usually consist of smaller droplets (e.g., Fig. 5). The single scattering albedo of the GOES SIR channel is 1% to 2% smaller than the 3.7-μm channels (Minnis et al. 1998), so the differences between the retrieved and actual values of r_e should be slightly larger than expected from the results of Nakajima and King (1990). The cloud droplet effective radii at cloud top are about 1–2 μm larger than the layer-mean values in this case as shown in Fig. 5, and within a few tenths of a micrometer of FSSP-measured values at cloud top. These differences are similar to those between retrieved and true values found by Platnick (2000) from theoretical calculations using realistic vertical profiles of droplet size for a stratus cloud with $\tau = 15$.

The variations of aircraft-derived LWP and optical

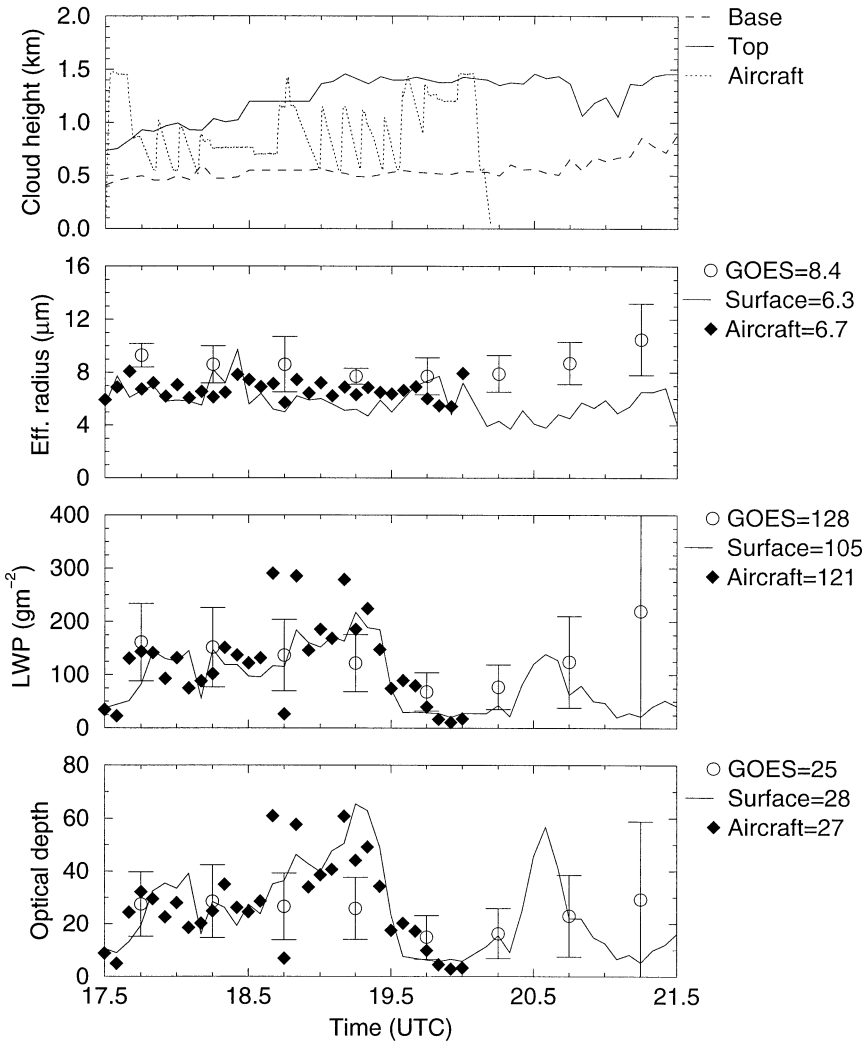

FIG. 4. The ceilometer-measured cloud-base height (dash) and radar-derived cloud-top height (solid), r_e, LWP, and τ vs time for 3 Mar 2000. The means given on the right of the panels represent the averaged values when all three datasets are available, such as from 17.5 to 20.0 UTC.

depth (τ) (Fig. 4) follow the trend of surface-derived values and the 2.5-h mean LWP is very close to the surface result. However, the variations in the individual satellite LWP retrievals do not closely follow the trend of the surface data. This is likely due to the spatial coverage of the satellite data. Each satellite data point in Fig. 4 represents the averaged value of ~150 pixels (4 km), while the surface data represent 5 min and about 3 km spatially averaged information. A larger time or space average would reduce the variability as shown in the study of Dong et al. (1998).

b. Case 2, 17 March

During case 2, the clouds moved from south to north at approximately 10 m s^{-1}, straddling the low-level inversion with temperatures between 1° and 4°C (Fig. 1b). A thin layer of cirrus at an altitude of ~9 km with a temperature of 220 K overlaid the stratus between 17.0 and 20.5 UTC. The flight primarily consisted of an ''S'' pattern flown over the SGP central and supplemental facilities (Fig. 2b). The ground-based ceilometer- and radar-derived cloud-base and -top heights are 0.3 and 1.7 km, respectively, while the aircraft flew at an altitude of approximately 1 km from 18.0 to 20.5 UTC (Fig. 6). Overall, the aircraft-derived effective radius agrees well with, and the LWP and optical depth are smaller than those from the ground-based data. The LWP and τ time series also disagree more than in the 3 March case. The surface-based retrievals depend primarily on the cloud LWP and the solar transmission. Since LWC generally increases with height within the cloud, we expect the surface retrievals to be more weighted by the cloud properties in the upper region of the cloud and the com-

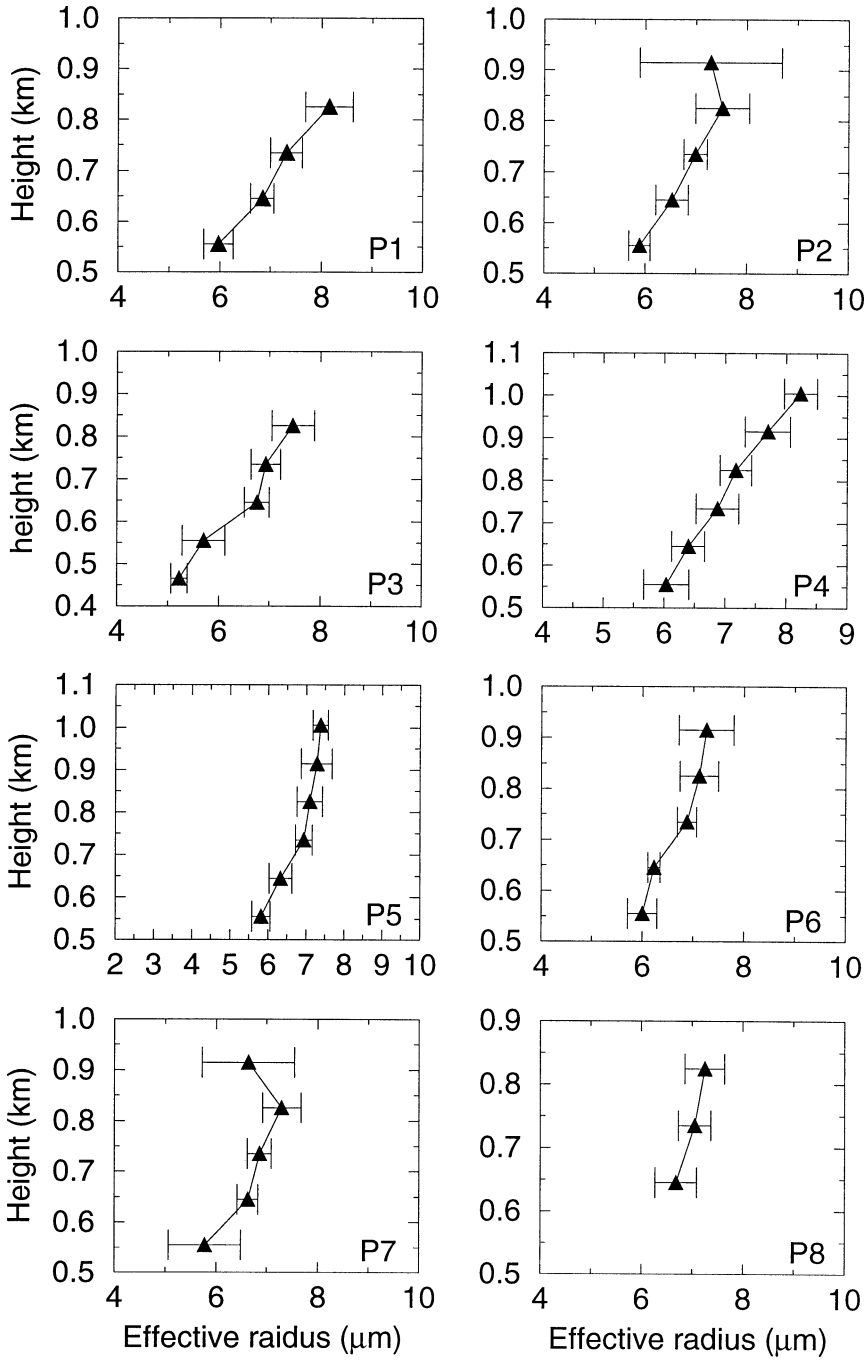

FIG. 5. Eight profiles of cloud droplet effective radius from aircraft FSSP data at the ARM SGP site on 3 Mar 2000.

parison with the aircraft-derived values to be best in the middle to upper region of the cloud layer where the conjunction of higher liquid water contents and large droplets occur (Dong et al. 1998).

The GOES-derived effective radius exceeds both the surface and aircraft results by 2 μm on average. When the cirrus cloud is thickest (between 17.5 and 18.5 UTC), the VISST-derived value of r_e is actually less than the value from the surface. Some of the FSSP values are as large as the VISST values even though the plane is in the middle of a 1.5-km-thick cloud. As the cirrus clouds leave after the 20.5 UTC, the VISST-derived r_e remains 2–3 μm larger than its surface-based counterpart even though the departure of the cirrus is marked by a 2–6-K rise in T_c. Unlike case 1, the GOES-derived optical depths are 15% less than the surface

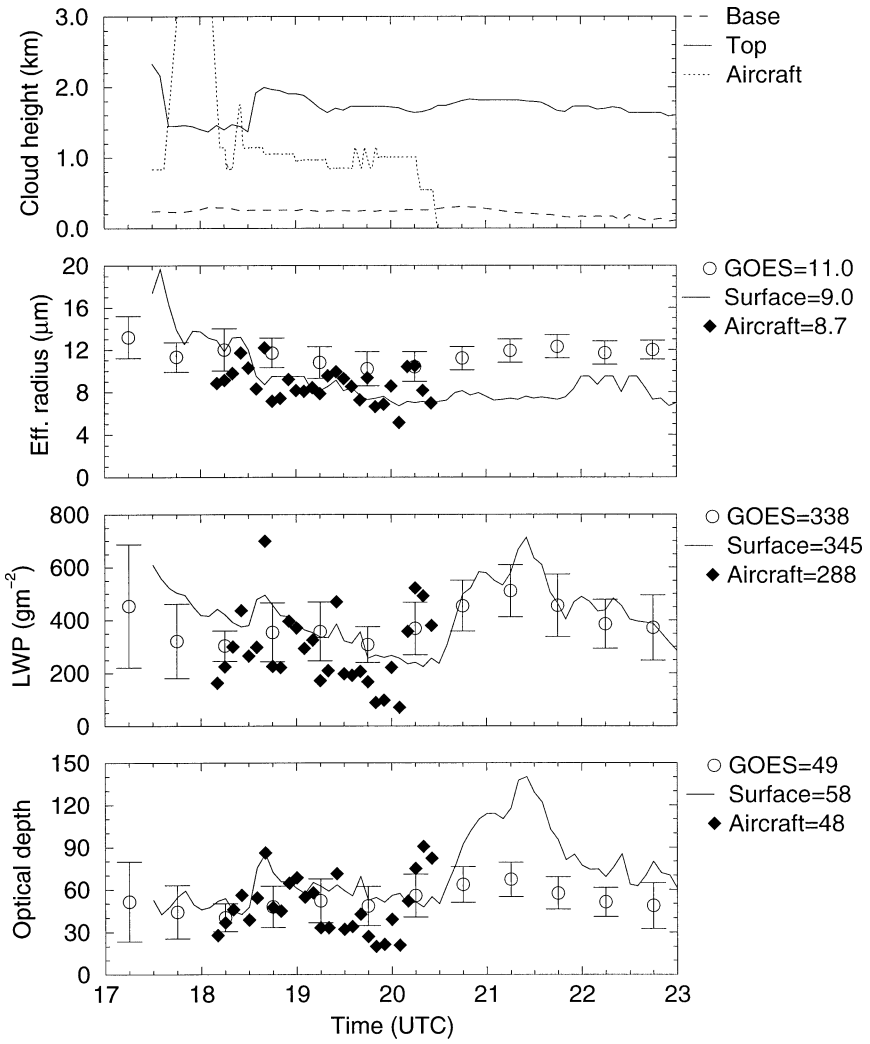

FIG. 6. Same as Fig. 4, but for 17 Mar 2000.

values, but agree with the aircraft results. The disagreement in τ continues after the cirrus clouds leave, but the surface- and VISST-derived LWP values are in good agreement because the small VISST optical depths are compensated by the large values of r_e. These results suggest that the cirrus clouds had little effect on the VISST retrievals for this case.

To estimate the impact of the cirrus on the retrievals, the VISST reflectance and emittance parameterizations were used to compute values of T_{SI}, T_{IR}, and T_{SWC} for a range of ice crystal sizes with $T_c = 220$ K and the observed cirrus-free values west of the SCF using the angles at 1745 UTC. The mean observed IR temperatures over and west of the SCF are 266 and 272.5 K, respectively, with corresponding r_e values of 10.5 and 11.0 μm. To facilitate a retrieval, the cloud underneath the cirrus is assumed to have the same properties as the low cloud deck west of the SCF. The best match with the observed values over the SCF was found for a cirrus cloud at 220 K having $D_e = 35$ μm and an optical depth of $\sim$0.25. The optical depths of the cirrus clouds were less than 0.2 during all of the remaining hours. Thus, it is concluded that the cirrus cloud increases the value of r_e by less than 0.5–1.0 μm for any of the hours for this case.

This apparently small effect of the cirrus cloud is supported by the differences between the values of r_e for the SCF cloud and the clouds to the west where no cirrus was apparent, as indicated by inspection of the imagery and the mean value of T_{IR}. Between 17.5 and 20.0 UTC when cirrus was present over the SCF and $T_{\mathrm{IR}} < 272$ K, the mean value of r_e is 1.2 ± 1.4 μm greater than the mean value for the 0.5° box that is 2° directly west of the SCF and has no values of T_{IR} less than 272 K. Between 20.0 and 23.0 UTC, the mean values differ by 1.2 ± 0.9 μm and $T_{\mathrm{IR}} > 272$ K for all hours in both boxes. The greatest differences for the first and second periods are 2.6 and 2.3 μm, respectively. Thus, the cloud properties over the SCF were different than those further to the west in the same cloud

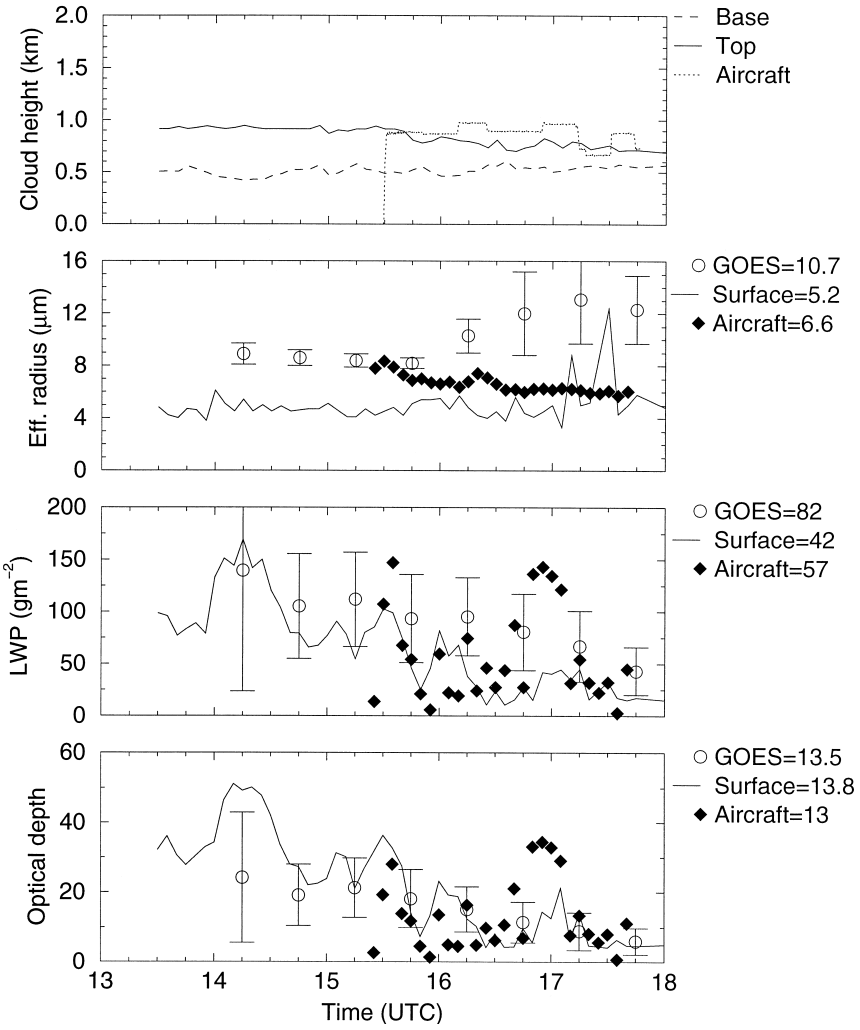

FIG. 7. Same as Fig. 4, but for 19 Mar 2000.

deck. These differences are similar to those between the surface and VISST. It is unfortunate that the aircraft was unavailable during that period to provide vertical profiles of r_e.

c. Case 3, 19 March

During case 3, the University of North Dakota aircraft was restricted by air traffic control to flight levels near cloud top so the flight pattern was designed to sample the turbulence and microphysical properties near cloud top. This required long level legs that were flown perpendicular and parallel to the flow. The cloud hovered below the lowest inversion at a temperature of about -2°C (Fig. 1c). The cloud elements advected from north to south at 20 m s^{-1}, while the entire cloud field propagated from west to east during the flight. As shown in Fig. 7 and Fig. 3c, the cloud was solid early in the morning with cloud-base and -top heights of 0.5 and 1 km, respectively. It gradually became thin with fluctuating base and top heights. The cloud layer began breaking up and finally dissipated and moved out by noon. No cirrus clouds were observed in the satellite or radar imagery. In this case, most of the in situ effective radii are greater than the surface retrievals (Fig. 7) presumably because the aircraft flew near cloud top. The aircraft-derived cloud LWP and τ scatter around the surface results despite the offset in r_e. Although the aircraft flew over the site during much of the flight, it was nearly 100 km away from the SCF at times, making it difficult to draw any firm conclusions from this comparison. However, it is encouraging that the average surface-retrieved optical depths and effective radii during the 2-h flight period are close to the aircraft results.

The GOES-derived τ values agree well with surface results and the satellite-derived LWPs have the same trend as the surface data but with much higher mean values. The GOES-derived r_e values are consistently larger than the surface results for the entire period and become progressively larger when the cloud layer

breaks up near the end of the period. The in situ effective radii are nearly the same as the VISST retrievals between 15.25 and 15.75 UTC prior to the breakup of the cloud layer. The increased particle size in the satellite-derived data near the end of the period is mainly due to the inclusion of partly cloudy pixels in the averages and to cloud inhomogeneities. The satellite-derived cloud fraction for the box was 100% until 17.25 UTC when it dropped to 88%. At 17.75 UTC, the cloud fraction decreased to 64%. Detailed examination of the satellite results from 17.25 UTC revealed that r_e varied between 9 and 10 μm in the lower right-hand corner of the 0.5° box, while r_e for the broken cloud pixels was closer to 20 μm, giving the large average at 17.25 UTC. As shown by Han et al. (1994), partially cloud-filled pixels reduce the apparent SI radiance causing an overestimate of r_e. Nguyen et al. (2002) estimated the cloud fraction within each 4-km pixel using the GOES 1-km VIS data for the 19 March case and found that between 16.25 and 17.75 UTC, r_e is 1–3 μm less than the values shown in Fig. 7 when partially filled pixels are taken into account. Another factor that may be causing some bias is the morphology of the cloud field. A periodic light–dark structure is evident in the 1-km visible imagery (not shown). At 16.25 UTC, both T_c and its standard deviation increased also suggesting structural changes in the cloud deck. The radar data and the variability in the downwelling shortwave radiation at the surface suggest that the layer became very inhomogeneous after 16.0 UTC possibly breaking into individual cloud cells. The changes in r_e after 17.0 UTC are highly erratic resulting in values as great as 12 μm. Periodic variations are also evident in the surface LWP and in the undulations of cloud-base and -top heights after 15.75 UTC (Fig. 7). This characteristic of the cloud field may cause 3D effects that diminish the validity of the plane parallel assumption made in the retrievals. Cloud inhomogeneity may have significantly biased the retrievals from both the surface and satellite in this particular case.

d. Case 4, 21 March

Although only a few scattered cirrus clouds passed over the SCF, the cloud properties from case 4 are much more complicated than the other three cases because multiple low-cloud layers occurred during the flight. As Fig. 3d and the ground-based radar observation illustrate, there are thin and broken cirrus clouds around the site from 1500 to 2100 UTC but these thin and broken cirrus do not affect either the surface or GOES stratus retrieval results significantly as discussed below. The 17.5 UTC sounding indicates that the low-level stratus cloud advected northward at ~10 m s^{-1} in a southerly flow under a strong inversion at 3.2 km. The cloud temperature varied from −3°C at cloud top to 10°C at cloud base (Fig. 1d). As in case 2, the Citation flew mostly within 20 km of the SGP central facility in an S pattern during the 2.5-h period (Fig. 2d).

The mean surface-retrieved r_e, LWP, and τ during the 2.5-h flight period are in excellent agreement with those derived from the in situ measurements (Fig. 8). However, some aircraft results, compared to surface retrievals during certain time periods, are opposite to the comparisons in the three other cases. For example, the in situ measured r_e values are smaller than the surface retrievals from 17.7 to 18.0 UTC period when the aircraft flew near cloud top. When the aircraft was near cloud base (18.3 to 18.7 UTC), the in situ sizes are much larger than the surface results. Additionally, a cloud layer detected by the aircraft probes from 18.9 to 19.4 UTC was above the highest cloud level observed by the surface-based remote sensors at the SGP central facility. This cloud layer is actually in the radar plot (Fig. 9) but was tossed out in the cloud screening and in the plot of cloud top in Fig. 8. The cloud-top height shown in Fig. 8 from 18.9 to 19.4 UTC was the cloud top of the lower layer. More than one distinct cloud layer may alter the assumed profile of monotonically increasing particle size with cloud height causing the type of comparisons seen in Fig. 8. To better explain these anomalies, the vertical profiles of radar reflectivity, cloud LWC, and r_e derived from the surface (Fig. 9) as in Dong and Mace (2002) are examined in detail. The results in Fig. 9 were derived using the following information. The inferred r_e profile is proportional to the layer-mean cloud droplet effective radius derived as in D97 and to the ratio of radar reflectivity to integrated radar reflectivity. The accuracy of inferred cloud droplet effective radius is the same as that for the D97-derived layer-mean r_e (~10%). The cloud-base height obtained from the laser ceilometer is used to identify cloud base in the radar returns. The microwave radiometer-derived LWPs are used as a constraint on the vertical sum of the derived cloud liquid water contents.

Two different cloud layers are apparent in Fig. 9. The cloud-base and -top heights of the lower layer are around 0.5 and 1.5 km, respectively, at 17.0 UTC. After 17.5 UTC, the cloud-base height increases and cloud-top height remains nearly constant. By 19.0 UTC, the lower layer merged with the upper layer. The cloud-base and -top heights of the upper layer are approximately 1.5 and 3 km, respectively, at 17.0 UTC. This upper layer starts to break up at 17.5 UTC. The base of the upper layer is gradually replaced or merged with the lower layer, while its top part forms a 100–200-m-thick layer at 18.5 UTC. This thin upper layer is apparently the one sampled by the aircraft around 19.0 UTC. As Fig. 9 illustrates, the cloud microphysics of two layers are quite different. The retrieved cloud LWC and r_e values of the upper layer are relatively uniform but much smaller than those in the lower layer. The retrieved LWC and r_e profiles from the lower layer, which decrease with height, are very different from our conceptual model. Considering Figs. 8 and 9 together, it can be seen that

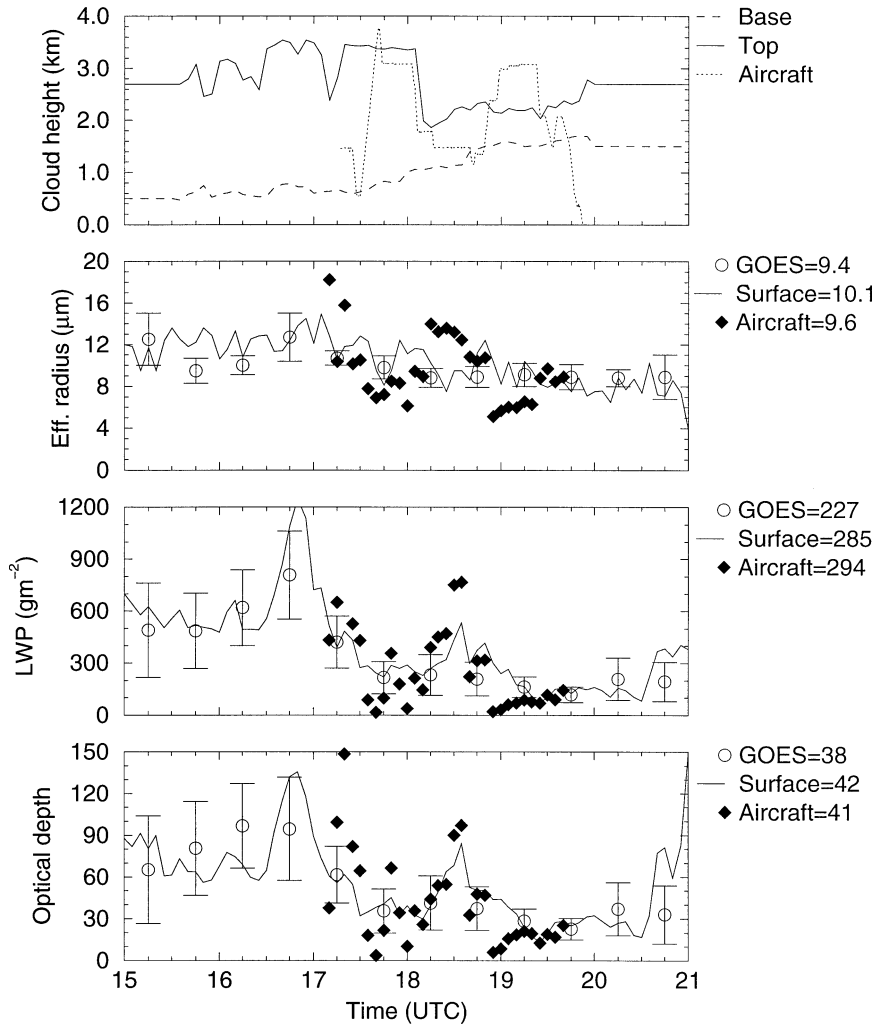

FIG. 8. Same as Fig. 4, but for 21 Mar 2000.

the aircraft in situ observations during the three time periods mentioned above are nearly identical to the surface retrievals. For instance, the aircraft-measured r_e and LWC values are approximately 1) 7 μm and 0.1 g m^{-3} at the cloud height of 3 km from 17.7 to 18.0 UTC, 2) 13 μm and 0.1 g m^{-3} at the cloud height of 1.5 km from 18.3 to 18.7 UTC, and 3) 6 μm and 0.1 g m^{-3} at the cloud height of 3 km from 18.9 to 19.4 UTC.

Consistent with the radar plots (not shown), the VISST results show some cirrus clouds at 15.25 and 16.75 UTC. Cirrus clouds account for ~25% of the cloud cover at 19.75 and 20.75 UTC. The dissipation of the upper stratus layer is reflected in the rise in T_c from ~268 K at 17.25 UTC to ~272 K at 17.75 UTC. The VISST-derived LWP and τ values during the entire period have almost the same trends as the surface retrievals, but the mean LWP and τ are 20% and 10% less, respectively, than the surface values during the flight period. Since the GOES-derived r_e is heavily weighted by the droplet sizes in the upper layer, the GOES-derived r_e values in this case are slightly less than the layer-mean surface retrievals. At 16.75 UTC, the GOES-derived r_e reaches the maximum value, which is consistent with the surface radar retrievals as shown in Fig. 9. The cirrus clouds are apparently well screened by the VISST phase determination, as there appears to be no cirrus contamination of the GOES-derived effective radii based on the type of criteria discussed for case 2. The large standard deviations in the VISST optical depths indicate considerable variation of the values within the 0.5° box. In nearly all cases, the surface-based optical depth is within one standard deviation of the satellite retrieval.

e. Summary of the four in situ cases

To match the GOES temporal resolution (30 min), the 5-min surface and aircraft data were averaged to 30-min means. Figure 10 shows the scatterplots of the half-hourly averages for the three datasets for the combined

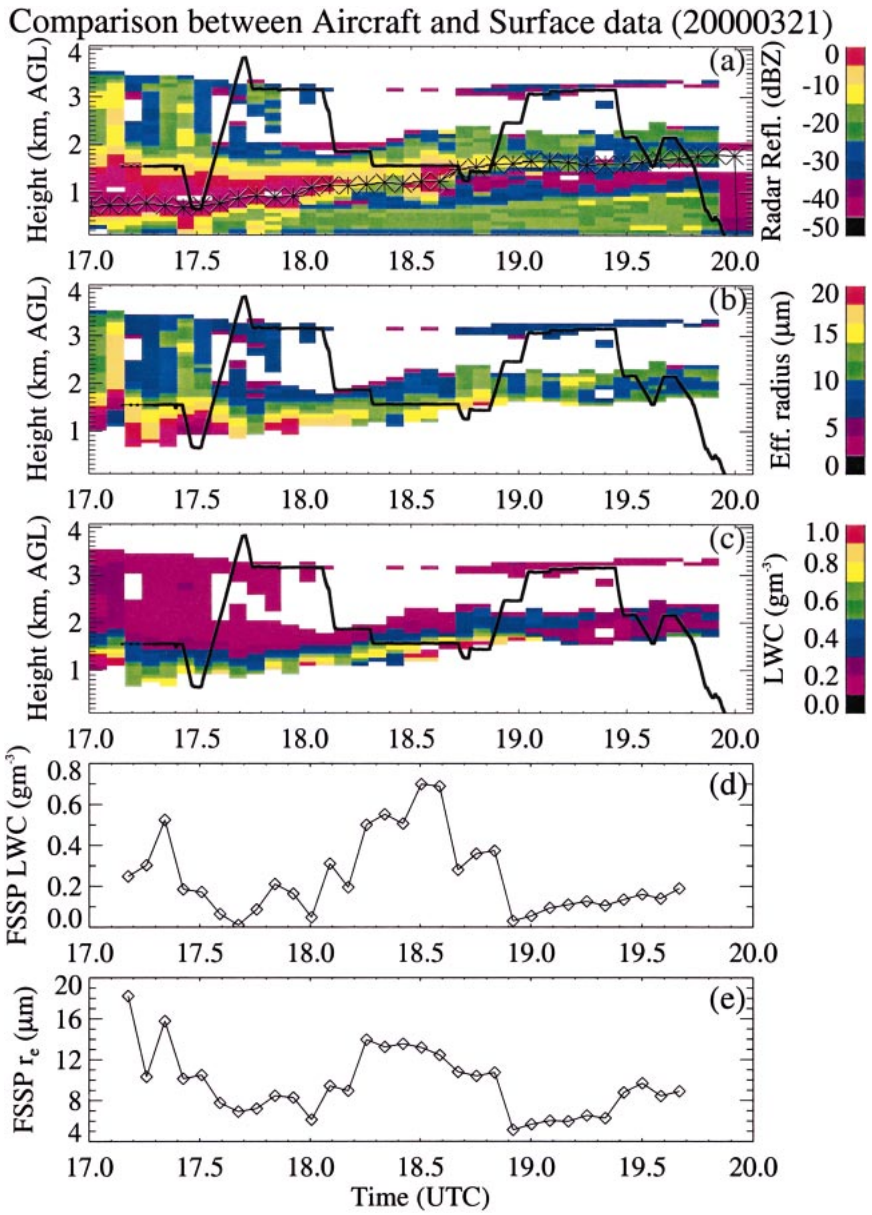

FIG. 9. (a) Radar reflectivity with ceilometer-measured cloud-base height (asterisks), (b) cloud r_e, and (c) LWC profiles (5 min). Aircraft altitude (solid line) in (a), (b), and (c). (d) The 5-min averages of cloud LWC and (e) r_e from the aircraft FSSP data.

10 h of in situ data. The means and standard deviations (SD) of the differences and the correlation coefficients of the surface and GOES retrieved r_e, LWP, and τ relative to the aircraft results are listed in Table 1 based on 22 30-min samples. The mean differences range from -4% to 23%, while the SD values vary from 20% to 41%, and their correlation coefficients are relatively large ($=>0.8$) except for the GOES-derived r_e. Most of the GOES-derived r_e values are larger than the surface and aircraft results, and their mean for the 10-h period is 2 μm larger than surface and aircraft means. This is consistent with the results in Fig. 5 and the conclusions of Nakajima and King (1990). The relatively poor (0.18) correlation coefficient between GOES and aircraft r_e shown in Table 1 is primarily a result of the last three data points derived from GOES during the 19 March case (Fig. 7). When these broken cloud cases are not included, the data line up much more closely (correlation coefficient = 0.55), and the mean difference in r_e is reduced by 1.0 μm bringing all of the results into closer agreement. There is excellent agreement in cloud LWP and τ and almost the same mean values from all three datasets for the 10-h period. Overall, for the entire 10-h period the surface retrievals have ex-

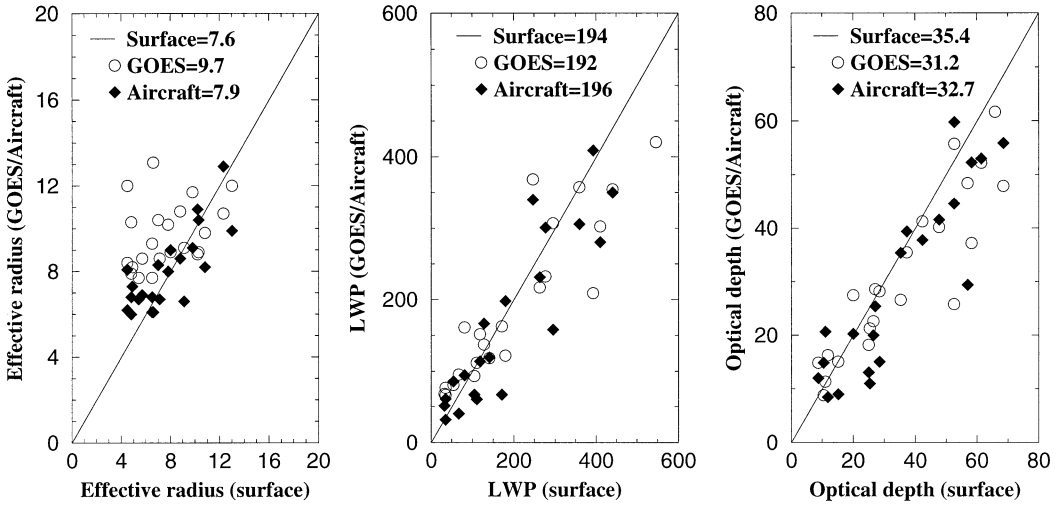

FIG. 10. Comparison of r_e, LWP, and τ from the GOES, aircraft, and surface datasets from the four in situ cases during the 10-h period (30-min resolution).

cellent agreement with the aircraft data, and the GOES results agree reasonably well with the surface and aircraft data in spite of the large differences in temporal and spatial sampling.

Other potential sources of error in the satellite retrievals include the use of relatively low-resolution rapid update cycle (RUC) profiles of humidity and temperature and the calibration of the visible channel. The satellite retrievals were repeated using the actual 3-hourly soundings from the SCF interpolated in time. The results were not significantly different from those using the RUC profiles. Use of the Moderate Resolution Imaging Spectroradiometer (MODIS) calibration for GOES instead of VIRS (see Minnis et al. 2002) would increase the optical depths. However, the MODIS calibration is provisional at the time of this writing. Other errors may be introduced by the interpolation of the 3.9-μm reflectance lookup tables. Structure in the model reflectance fields that occurs between the model nodes will be missed in the retrieval because the interpolation smoothes out the variations. Increased resolution in the lookup tables would be needed to reduce the interpolation errors.

The 5-min averages of r_e and LWC from the aircraft FSSP data may not well represent the whole cloud layer. Some of these averages might be smaller (larger) if the aircraft was in the lower (higher) part of cloud during the 5-min averaging period than the surface layer-mean results. However, for longer time periods, the averages should represent the true values for both surface and aircraft because the horizontal and vertical variability will be well sampled. A previous study demonstrated that averaging both the aircraft and surface data to 30-min resolution significantly reduces their mean differences, suggesting that both the aircraft and surface data are capable of characterizing the cloud microphysics over this temporal scale (Dong et al. 1998). From sampling theory, it is estimated that the expected errors in the mean LWP and τ from the surface and aircraft data for the 22 samples are 3% or less. Thus, the agreement in the mean values of LWP from all three platforms may not as close as the 1%–2% found here, but should be within $\pm 5\%$.

The aircraft-derived LWP and τ values further complicate this issue because these values are derived from aircraft-measured LWC and surface-measured cloud thickness. The best sampled cloud profiles during the IOP were taken on 3 March, but even these profiles were not gathered directly above the ground-based instrument, do not always start from cloud top or end at cloud bottom, and did not last for 5 min. Nevertheless, a comparison of the 3 March in situ profiles to the surface or GOES data does not make any notable difference in the analysis results. Because the 17, 19, and 21 March cases had fewer aircraft profiles, the aircraft-derived LWP and τ values are likely to scatter around the surface results more than the 3 March case, but they should still represent the whole cloud layer when averaged over 30-min or longer periods.

The average τ values from the surface are greater than both the aircraft and the satellite results. The surface-

TABLE 1. The means and standard deviations of differences and correlation coefficients (corr) of surface and GOES retrievals relative to aircraft results during the four in situ cases.*

	Surface			GOES		
	Mean (%)	SD (%)	Corr	Mean (%)	SD (%)	Corr
r_e	−3.8	20.1	0.78	22.8	25.4	0.18
LWP	−1.0	31.2	0.92	−2.0	40.8	0.85
τ	8.3	29.3	0.89	−4.6	29.5	0.87

* SD is calculated from square root [(rms)^2 − (mean difference)^2], and rms and mean difference are in percent relative to the aircraft averages.

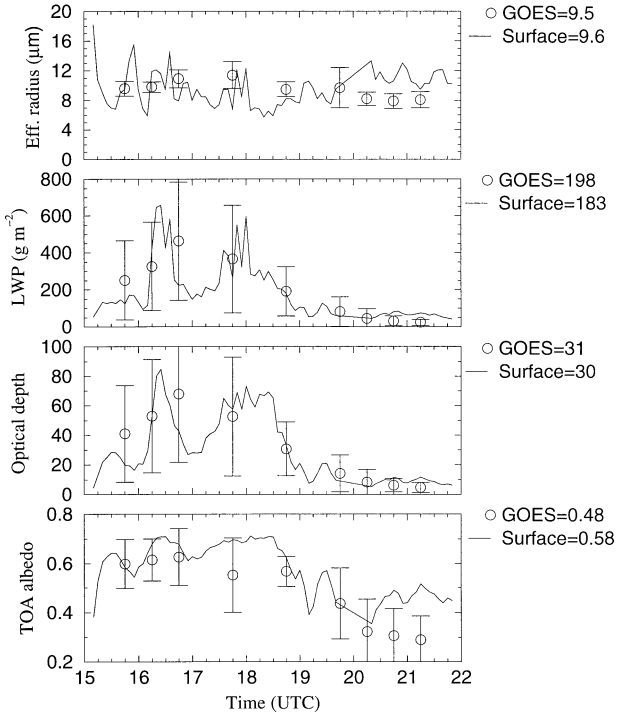

FIG. 11. Mean values of r_e, LWP, τ, and R_{TOA} for the GOES and surface datasets from 15.0 to 22.0 UTC 14 Mar 2000, the whole time period.

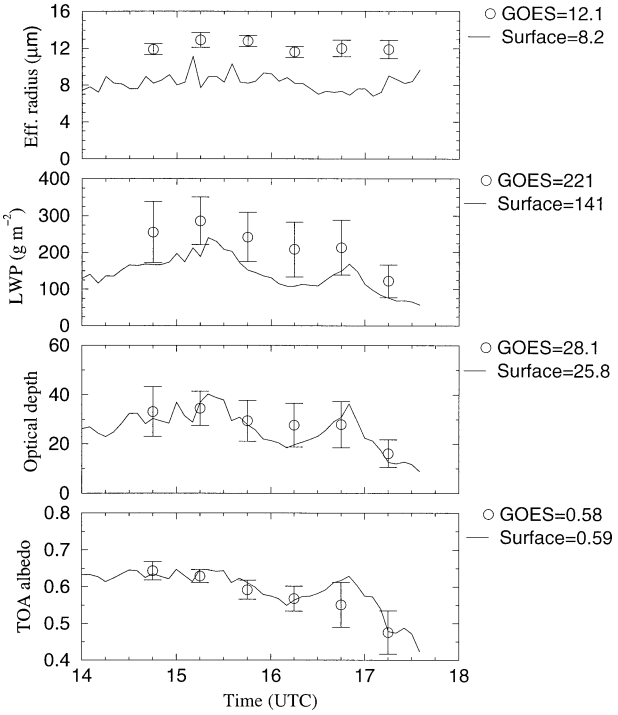

FIG. 12. Same as Fig. 11, but for 15 Mar 2000.

derived value is based on a broadband optical depth, which is that optical depth required to account for transmission of all of the solar radiation. The satellite value is define at a wavelength of 0.65 μm. Typically, the near-infrared extinction efficiencies for most cloud droplets are larger than their visible spectrum counterparts leading to a larger near-infrared optical depth for a given visible optical depth. For example, for $r_e = 10$ μm, the extinction efficiencies at 0.65 and 2.5 μm are 2.1 and 2.2, respectively (Fig. 3 of Dong 1996), and at 3.7 μm the extinction efficiency for $r_e = 8$ μm is 13% greater than the 0.65-μm value. Thus, the broadband optical depth, which is essentially a value convolved with the incoming solar radiation over the visible and near-infrared spectra, should in general be larger than the value at 0.65 μm. The exact difference between the broadband and visible τ will depend on r_e and the cloud thickness. Although it will probably not explain all of the difference in τ seen in Fig. 10, this spectral effect indicates that the two values should not be equal.

f. Three more cases and summary of seven cases with surface and GOES data only

The GOES-derived r_e, LWP, τ, and broadband TOA albedo (R_{TOA}) from three additional cases (14, 15, and 29 March) are compared in Figs. 11–13 with those deduced from the ground-based measurements. The GOES-derived r_e values generally agree with the surface

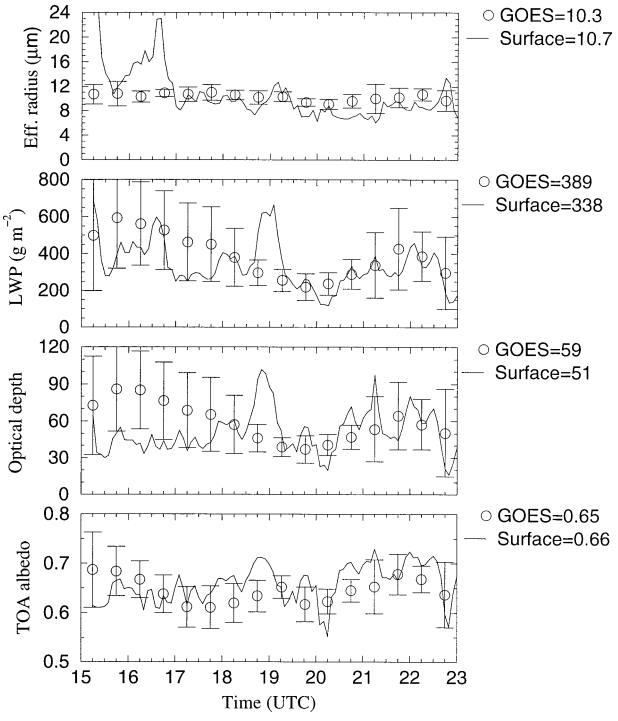

FIG. 13. Same as Fig. 11, but for 29 Mar 2000.

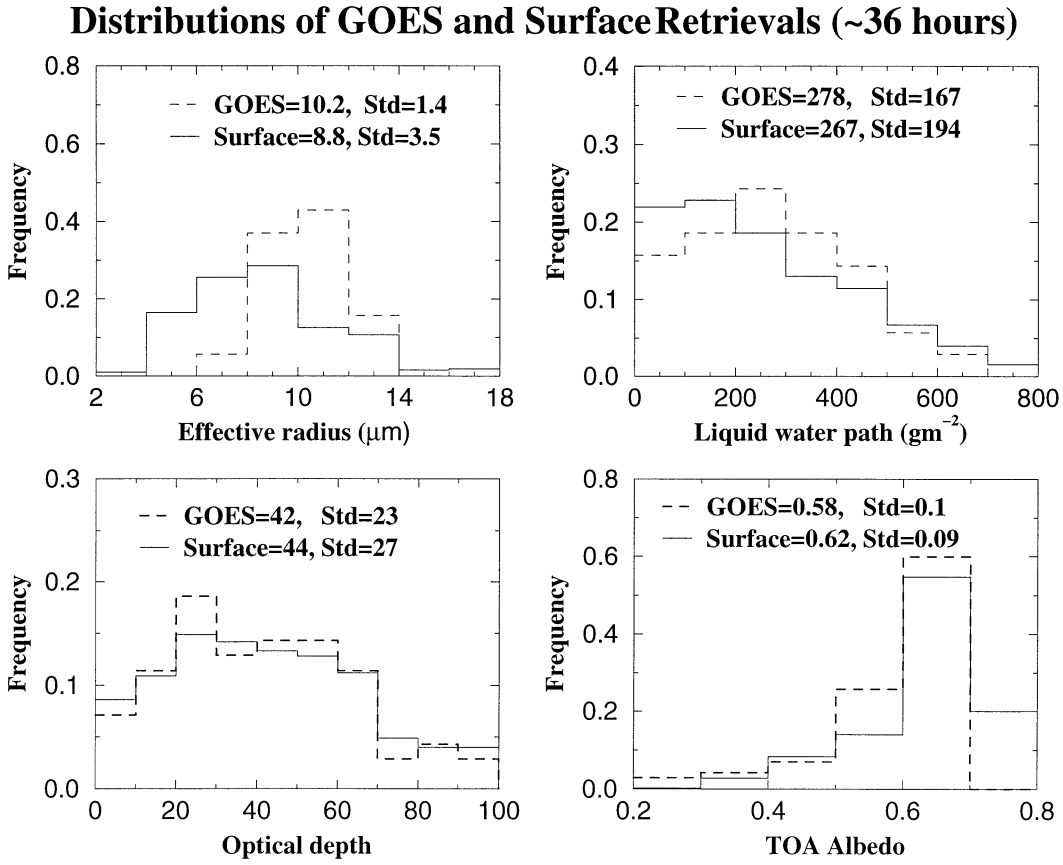

FIG. 14. Frequency distributions of surface (5 min) and GOES (30 min) r_e, LWP, τ, and R_{TOA} values during 36 h from seven cases during the IOP.

results except on 15 March, and have reduced variability compared to surface retrievals due to the larger spatial averages. Between 20.0 and 21.5 UTC, 14 March, the cloud fraction from the satellite varied between 60% and 90%. In this case, however, the value of r_e appeared to be unaffected by the breakup, presumably because the edge of the cloud field passed through the box. Instead of many partially filled pixels as seen during the 19 March case, most of the pixels were either completely cloudy or clear. The r_e values derived from GOES data are much larger than those derived from surface retrievals (~50%) on 15 March. Several reasons that might cause this difference were investigated but failed to explain the bias on that particular day. First, the brightness temperature differences between the 3.9- and 11-μm channels in the 0.5° box are much smaller on 15 March compared to the 21 March, which indicates that the solar reflection part in the 3.9-μm channel is small and r_e should be larger on the 15 March. Second, the soundings used for satellite atmospheric corrections agree well with those from the radiosondes. Third, the largest r_e retrieved from the ground-based radar and microwave radiometer measurements is around 10 μm during the entire period. Therefore, the conflicting surface and satellite values remain unresolved. Other possible sources for the discrepancy, such as the calibration of the surface instruments, will be examined at a later time.

The two optical depth datasets are mostly in good agreement, with a few exceptions, such as in Fig. 13. The comparison of LWP from the two datasets is similar to that of τ, and has a similar pattern of variability from 14 and 29 March. However, the LWPs derived from GOES data are much larger than those derived from the surface on 15 March due to the large particle size retrieved from GOES. The broadband TOA albedos from GOES are slightly smaller than those from the surface except for a few points as seen in Fig. 11. This small difference may be due to any of the following reasons: 1) the GOES visible channel calibration, 2) variable anisotropy in the GOES-viewed radiances, 3) the satellite narrowband-to-broadband conversion, 4) surface measurement and retrieval uncertainties, and 5) spatial sampling differences.

The frequency distributions of r_e, LWP, τ, and R_{TOA} from all seven cases with a total of 36 h of surface and GOES data during the IOP are illustrated in Fig. 14. The temporal resolutions are 5 min for surface data and 30 min for GOES in these histograms. Most of surface-retrieved r_e values range from 4 to 14 μm with the mean and standard deviation of 8.8 and 3.5 μm, respectively.

The range of GOES-derived r_e values is narrower than that for the surface distribution and shifts to higher values due to the large spatial domain and the sensitivity to conditions at cloud top. The mean of r_e from GOES is about 1.4 μm larger than the surface mean, while the standard deviation is smaller. The GOES standard deviation is consistent with averaging over a larger spatial area. Nearly 45% of the cloud LWPs retrieved from ground-based microwave radiometer measured brightness temperatures are less than 200 g m^{-2} with a long tail toward higher values. The GOES-derived LWPs have a similar distribution with a slightly higher modal frequency between 200 and 300 g m^{-2}. The means and standard deviations of LWPs from two datasets are nearly same as seen in Fig. 14. The frequency distributions, means, and standard deviations in τ from two datasets are almost the same. Most τ values range between 10 and 70. The mean values for R_{TOA} from surface and GOES are 0.62 and 0.58, respectively, with a frequency of occurrence modal value of 0.65.

Given the large spatial (3 km versus 50 km) and temporal (5 min versus 30 min) resolution differences between the surface and GOES, as well as the uncertainties in the measurements and retrievals from the two datasets, the broadband R_{TOA}, τ, LWP, and r_e comparisons are very encouraging despite the existence of some unresolved discrepancies. The date, time period, means, standard deviations of the differences, and correlation coefficients of r_e, LWP, τ, and R_{TOA} from the two datasets for each case are listed in Table 2 to summarize the comparison between surface and GOES retrievals. Based on all samples, the means and SDs of the differences of the GOES-derived r_e, LWP, τ, and R_{TOA} relative to the surface retrievals are 16% $\pm$ 31.2%, 4% $\pm$ 31.6%, $-$6% $\pm$ 39.9%, and $-$6% $\pm$ 6.1%, respectively. The respective correlation coefficients are 0.24, 0.88, 0.73, and 0.91. For each individual case, the SD of the differences can be as large as 44%, and the correlation coefficients can be negative or positive. These results reveal that further study is necessary to explain the various instantaneous differences.

Figure 14 provides substantial evidence that the mean results from a 0.5° box consisting of ~150 pixels are equivalent to those from a 30-min average of cloud elements advecting over the surface site. Because of uncertainties in actual locations of clouds viewed by the various surface instruments and in the locations of the satellite pixels relative to the surface-viewed areas, it is not clear that this approach is optimal for comparing the two datasets. Two additional datasets were constructed from the GOES pixel-level results to examine the sensitivity of the comparison to the spatial and temporal sampling. The first uses the so called ''wind strips,'' based on the wind velocity at cloud top. The mean values of each parameter were computed using only those pixels in a line centered on the SCF that covers the distance a parcel near cloud top would travel in 0.5 h. Considering that most of the radiation observed

TABLE 2. The means, standard deviations (SD) of differences, and correlation coefficients (corr) of surface and GOES data from seven cases during the IOP.*

Date	Time (UTC)	r_e(μm)				LWP (g m^{-2})				τ				TOA albedo			
		Surface	GOES	SD (%)	Corr	Surface	GOES	SD (%)	Corr	Surface	GOES	SD (%)	Corr	Surface	GOES	SD (%)	Corr
3 Mar 2000	17.5→21	5.8	8.4	14.1	0.28	94.8	120	41.0	0.6	26.6	23.2	42.4	0.65	0.57	0.54	8.0	0.82
14 Mar 2000	15.5→21.5	9.9	9.5	21.7	−0.57	182.2	198	38.7	0.89	28.4	30.9	37.2	0.88	0.57	0.48	9.6	0.92
15 Mar 2000	14.5→17.5	8.2	12.2	7.5	0.65	145.5	221	11.7	0.96	26.6	28.1	10.0	0.92	0.59	0.58	4.2	0.95
17 Mar 2000	17.5→23	9.3	11.4	27.3	0.19	421.6	380.9	18.6	0.6	71.7	52.4	22.5	0.83	0.68	0.65	3.1	0.87
19 Mar 2000	14→18	5.2	10.2	30.3	0.7	77.4	92	20.0	0.95	20.8	15.5	33.8	0.93	0.53	0.49	6.3	0.98
21 Mar 2000	15→21	10.4	9.9	13.4	0.66	399.1	347.3	19.1	0.94	55.9	52.8	30.5	0.76	0.66	0.62	4.1	0.74
29 Mar 2000	15.5→23	10.1	10.2	25.3	0.54	334.9	381.7	32.2	0.46	51.7	58.2	43.6	−0.3	0.66	0.64	4.2	0.34
Total	~36 h	8.8	10.2	31.2	0.24	267.3	278	31.6	0.88	44.3	41.7	39.9	0.73	0.62	0.58	6.1	0.91

* SD is calculated from square root [(rms)^2 −(mean difference)^2], and rms and mean difference are in percent relative to the surface averages.

TABLE 3. Mean cloud properties and correlation coefficients (corr) for different matching conditions.

	r_e (μm)	Corr	LWP (g m^{-2})	Corr	τ	Corr
Surface, 5 min	8.8		258.5		43.0	
Small box	10.2	0.10	259.5	0.69	38.8	0.59
Surface, 30 min	8.8		267.3		44.3	
Wind strip	10.2	0.19	270.1	0.85	40.0	0.66
0.5° box	10.2	0.24	278	0.88	41.4	0.73

by the shortwave radiometer is received at zenith angles less than 75°, the radius of the field of view would be approximately 3.7 km for a cloud base at 1 km. Thus, the line of GOES data was assumed to be two pixels wide. An extra pixel was included at the end of the line to account for the uncertainty of the center of line compared to the location of the SCF (pixel centers and edges do not usually coincide with a given grid). The number of 4-km GOES pixels determined in this fashion varied from 8 to 16 depending on the wind speeds. These data are compared to the 30-min averages from the surface. The second dataset, a small box consisting of the mean values for a 3×3 pixel array centered on the SCF, is compared to the 5-min averages at the time of satellite image.

The results are summarized in Table 3, which shows the mean values for all of the data and the linear correlation coefficients from regression of the various satellite and surface datasets. Mean effective radius is the same for all of the satellite datasets and exceeds the corresponding surface values by 1.4 μm. The small box and wind strip values of τ are noticeably smaller than the 0.5° box mean resulting in a larger underestimate compared to the surface-derived optical depths. However, the mean LWP values from the wind strip and small box are closer to the surface-derived value than the mean from the 0.5° box. All of the correlation coefficients for the 0.5° box exceed those from the wind strip and small box data. These results indicate that a comparison of 0.5° box data with half-hourly averaged surface-based data is as good as or better than using more detailed data matching. It should be noted that this analysis was confined to low clouds. Because high clouds move faster and correspond to a larger field of view from the surface radiometer, average values from larger boxes may be better for comparisons with high clouds.

4. Conclusions

The March 2000 ARM cloud IOP was a very successful field experiment with a wide variety of cloud types observed during the 4-week period. Four low-level stratus cases (10 h) were intensively observed by ground- and satellite-based remote sensors and aircraft in situ instruments. The results show that the surface-based technique can reproduce the bulk properties of the stratus cloud to within 20%–30% of the values derived from the aircraft data on a relatively instantaneous (30-min average) basis. On average, the surface retrievals are unbiased relative to the aircraft in situ results. In a similar fashion, these comparisons show that the satellite retrieval also produces statistically unbiased values of liquid water path and optical depth that are within 25% to 40% of the aircraft data for a given retrieval. The GOES-derived droplet sizes exceed the aircraft values by 2 μm or 23%, on average, with a standard deviation close to that seen for the surface–aircraft comparisons.

Three additional stratus cases were examined using only the surface and satellite data. Combining the results with those from the aircraft study produced a total of 36 h of matched data. The mean satellite-derived cloud optical depth is 5.8% $\pm$ 4.0% less than the surface-derived mean, while instantaneous differences are similar to those for the satellite-aircraft comparisons. Mean liquid water path derived from GOES is statistically the same as that from the surface, although individual values typically differ by 30%. The mean effective droplet radius from GOES is 1.4 μm or 16% larger than its surface-based counterpart. This size difference is statistically significant. Some of the differences in effective droplet size can be explained by variations in the vertical profile of droplet sizes in the clouds and, in one case, by the presence of broken clouds. Cloud droplet size does not necessarily increase monotonically with altitude in stratus cloud systems because a given system may contain closely spaced, but distinct multiple layers. The reasons for the differences between the aircraft/surface and satellite effective droplet sizes were not discernable in several cases indicating the need for more detailed examination of the cloud physical structure.

It was demonstrated that spatial averages of satellite retrievals over a 0.5° region matched to half-hourly means from the surface could be used in lieu of more exact matching of the temporal data with the spatial data. This finding facilitates comparisons of long-term datasets because labor intensive detailed matching of the data is not necessary. Because of the larger area in the surface radiometer field of view and the generally greater wind speeds at high altitudes, pixels from a larger region may be needed for comparisons of satellite and surface retrievals for high clouds. Although the results from the two platforms are quite close on average, some outstanding discrepancies need further investigation to determine their cause. The overall good comparison between surface-based, aircraft and satellite retrievals suggests that the current technique for deriving microphysical properties for overcast single-layer liquid phase clouds from GOES should produce statistics similar to those from a radar-radiometer method similar to that used here. Thus, the statistics for stratus clouds can be confidently derived over other areas that lack the ARM ground-based instrumentation. Additional analyses and more sophisticated surface retrievals are need-

ed to evaluate the GOES-derived microphysical properties for other cloud types.

Acknowledgments. Data were obtained from the Atmospheric Radiation Measurement (ARM) program sponsored by the U.S. Department of Energy (DOE) Office of Energy Research, Office of Health and Environmental Research, Environmental Sciences Division. Special thanks to Ms. S. Benson for processing the surface data, Dr. J. Liljegren for reprocessing the ground-based microwave radiometer data, and three anonymous reviewers who provided insightful comments and suggestions. During this study, all authors are involved in the IOP with either total or partial support from the ARM program. The first author is also supported by NASA CERES project.

REFERENCES

Baumgardner, D., 1983: An analysis and comparison of five water drop measuring instruments. *J. Climate Appl. Meteor.,* **22,** 891–910.

——, and M. Spowart, 1990: Evaluation of the Forward Scattering Spectrometer Probe. Part III: Time response and laser inhomogeneity limitations. *J. Atmos. Oceanic Technol.,* **7,** 666–7672.

——, W. Strapp, and J. E. Dye, 1985: Evaluation of the Forward Scattering Spectrometer Probe. Part II: Corrections for coincidence and dead-time losses. *J. Atmos. Oceanic Technol.,* **2,** 626–632.

Dong, X., 1996: Microphysical and radiative properties of boundary layer stratiform clouds deduced from ground-based measurements. Ph.D. dissertation. The Pennsylvania State University, 132 pp.

——, and G. G. Mace, 2002: Profiles of low-level stratus cloud microphysics deduced from ground-based measurements. *J. Atmos. Oceanic Technol.,* in press.

——, T. P. Ackerman, E. E. Clothiaux, P. Pilewskie, and Y. Han, 1997: Microphysical and radiative properties of boundary layer stratiform clouds deduced from ground-based measurements. *J. Geophys. Res.,* **102,** 23 829–23 843.

——, ——, and ——, 1998: Parameterizations of microphysical and shortwave radiative properties of boundary layer stratus from ground-based measurements. *J. Geophys. Res.,* **103,** 31 681–31 693.

——, P. Minnis, T. P. Ackerman, E. E. Clothiaux, G. G. Mace, C. N. Long, and J. C. Liljegren, 2000: A 25-month database of stratus cloud properties generated from ground-based measurements at the ARM SGP site. *J. Geophys. Res.,* **105,** 4529–4538.

——, G. G. Mace, P. Minnis, and D. F. Young, 2001: Arctic stratus cloud properties and their effect on the surface radiation budget: Selected cases from FIRE ACE. *J. Geophys. Res.,* **106,** 15 297–15 312.

Dye, J. E., and D. Baumgardner, 1984: Evaluation of the Forward Scattering Spectrometer Probe. Part I: Electronic and optical studies. *J. Atmos. Oceanic Technol.,* **1,** 329–344.

Han, Q., W. B. Rossow, and A. A. Lacis, 1994: Near-global survey of effective droplet radii in liquid water clouds using ISCCP data. *J. Climate,* **7,** 465–497.

Kawamoto, K., P. Minnis, and W. L. Smith Jr., 2001: Cloud overlapping detection algorithm using solar and IR wavelengths with GOES data over the ARM/SGP site. *Proc. 11th ARM Science Team Meeting,* Atlanta, GA, DOE. [Available online at http://www.arm.gov/docs/documents/technical/conf_0103/kawamoto-k.pdf.]

Liljegren, J. C., E. E. Clothiaux, G. G. Mace, S. Kato, and X. Dong, 2001: A new retrieval for cloud liquid water path using a ground-based microwave radiometer and measurements of cloud temperature. *J. Geophys. Res.,* **106,** 14 485–14 500.

Miles, N. L., J. Verlinde, and E. E. Clothiaux, 2000: Cloud-droplet size distributions in low-level stratiform clouds. *J. Atmos. Sci.,* **57,** 295–311.

Minnis, P., and W. L. Smith Jr., 1998: Cloud and radiative fields derived from *GOES-8* during SUCCESS and the ARM-UAV spring 1996 flight series. *Geophys. Res. Lett.,* **25,** 1113–1116.

——, P. W. Heck, and D. F. Young, 1993: Inference of cirrus cloud properties using satellite-observed visible and infrared radiances. Part II: Verification of theoretical cirrus radiative properties. *J. Atmos. Sci.,* **50,** 1305–1322.

——, and Coauthors, 1995a: Cloud optical property retrieval (Subsystem 4.3). Clouds and the Earth's Radiant Energy System (CERES) algorithm theoretical basis document, Volume III: Cloud analyses and radiance inversions (Subsystem 4). NASA Tech. Rep. RP 1376, 135–176.

——, W. L. Smith Jr., D. P. Garber, J. K. Ayers, and D. R. Doelling, 1995b: Cloud properties derived from *GOES-7* for the spring 1994 ARM Intensive Observing Period using version 1.0.0 of the ARM satellite data analysis program. NASA Tech. Rep. RP 1366, 59 pp.

——, D. P. Garber, D. F. Young, R. F. Arduni, and Y. Takano, 1998: Parameterizations of reflectance and effective remittance for satellite remote sensing of cloud properties. *J. Atmos. Sci.,* **55,** 3313–3339.

——, W. L. Smith Jr., and D. F. Young, 2001: Cloud macro- and microphysical properties derived from GOES over the ARM SGP domain. *Proc. 11th ARM Science Team Meeting,* Atlanta, GA, DOE. [Available online at http://www.arm.gov/docs/documents/technical/conf_0103/minnis-p.pdf.]

——, L. Nguyen, D. R. Doelling, D. F. Young, and W. F. Miller, 2002: Rapid calibration of operational and research meteorological satellite imagers. Part I: Evaluation of research satellite visible channels as references. *J. Atmos. Oceanic Technol.,* **19,** 1233–1249.

Nakajima, T., and M. D. King, 1990: Determination of optical thickness and effective radius of clouds from reflected solar radiation measurements. Part I: Theory. *J. Atmos. Sci.,* **47,** 1878–1893.

Nguyen, L., P. Minnis, W. L. Smith Jr., D. F. Young, P. W. Heck, A. D. Rapp, and M. M. Khaiyer, 2002: Use of multi-resolution imager data to account for partially cloud-filled pixels. *Proc. 12th ARM Science Team Meeting,* St. Petersburg, FL, DOE. [Available online at http://www.arm.gov/docs/documents/technical/conf_0204/nguyen_1.pdf.]

Ou, S. C., K. N. Liou, and B. A. Baum, 1996: Detection of multilayer cirrus cloud systems using AVHRR data: Verification based on FIRE II IFO composite measurements. *J. Appl. Meteor.,* **35,** 178–191.

Platnick, S., 2000: Vertical photon transport in cloud remote sensing problems. *J. Geophys. Res.,* **105,** 22 919–22 935.

——, and F. P. J. Valero, 1995: A validation of a satellite cloud retrieval during ASTEX. *J. Atmos. Sci.,* **52,** 2985–3001.

Stokes, G. M., and S. E. Schwartz, 1994: The Atmospheric Radiation Measurement (ARM) program: Programmatic background and design of the cloud and radiation test bed. *Bull. Amer. Meteor. Soc.,* **75,** 1201–1222.

Wielicki, B. A., R. D. Cess, M. D. King, D. A. Randall, and E. F. Harrison, 1995: Mission to planet Earth: Role of clouds and radiation in climate. *Bull. Amer. Meteor. Soc.,* **76,** 2125–2153.

Young, D. F., P. Minnis, W. L. Smith Jr., and D. P. Garber, 1997: A four-channel method for deriving cloud radiative properties from meteorological satellite data. *IRS '96: Current Problems in Atmospheric Radiation,* W. L. Smith and K. Stamnes, Eds., Deepak, 612–615.